

SI Appendix

Singlet Oxygen Mediated Iron-based Fenton-like Catalysis under Nanoconfinement

Zhichao Yang^a, Jieshu Qian^b, Anqing Yu^a & Bingcai Pan^{a,c,1}

a.State Key Laboratory of Pollution Control and Resource Reuse, School of the Environment, Nanjing University, Nanjing 210023, China. b. Jiangsu Key Laboratory of Chemical Pollution Control and Resources Reuse, School of Environmental and Biological Engineering, Nanjing University of Science and Technology, Xiao Ling Wei 200, Nanjing 210094, China. c. Research Center for Environmental Nanotechnology (ReCENT), Nanjing University, Nanjing 210023, China. ¹To whom correspondence should be addressed. E-mail: bcpan@nju.edu.cn. Tel: +86-25-8968-0390.

Table of contents

Part S1 Supplementary Discussion	4
Part S2 Supplementary Experimental Section.....	5
Text S1 The intermediate products detection by UHPLC/MS.....	5
Text S2 Calculation of the concentration of products	6
Text S3 Chemicals and materials	7
Text S4 The transfer of XRD patterns	7
Text S5 Evaluating the stability and reusability of Fe ₂ O ₃ @FCNT-H.....	8
Text S6 The operation methods for reactive intermediates analysis by ESR	8
Part S3 Supplementary Figures	10
Fig. S1. TEM images of (A) FCNT-L and (B) FCNT-H.	10
Fig. S2. STEM-HAADF images of (A) Fe ₂ O ₃ /FCNT-L and (B) Fe ₂ O ₃ @FCNT-H.	10
Fig. S3. ⁵⁷ Fe Mössbauer spectra of both Fe ₂ O ₃ /FCNT-L and Fe ₂ O ₃ @FCNT-H at room temperature.	11
Fig. S4. Raman spectra of the catalysts.	11
Fig. S5. The molecular mass spectra of the detected (A) C ₅ H ₆ O ₄ , (B) C ₄ H ₄ O ₃ , (C) C ₅ H ₆ O ₃ , and (D) FFA in negative ionization mode by UHPLC/MS.	12
Fig. S6. The kinetics of MB degradation in both Fe ₂ O ₃ @FCNT-H/H ₂ O ₂ system and Fe ₂ O ₃ /FCNT-L/H ₂ O ₂ system.	12
Fig. S7. TOC removal during MB degradation in both Fe ₂ O ₃ @FCNT-H/H ₂ O ₂ system and Fe ₂ O ₃ /FCNT-L/H ₂ O ₂ system.	13
Fig. S8. The degradation of MB in the different systems.	13
Fig. S9. MB removal under different conditions.	14
Fig. S10. The MB degradation kinetics under different solution pH in Fe ₂ O ₃ @FCNT-H/H ₂ O ₂ system.	15
Fig. S11. The effect of solution pH on (A) MB removal by Fe ₂ O ₃ /FCNT-L with/without H ₂ O ₂ and (B) degradation kinetics.....	16
Fig. S12. MB removal in xanthine-xanthine oxidase system.	16
Fig. S13. The inhibition efficiency of the catalytic activity of Fe ₂ O ₃ @FCNT-H using different quenching molecules.	17
Fig. S14. The effect of pH on HO ₂ •/O ₂ ⁻ and ¹ O ₂ generation.....	17
Fig. S15. (A) The adsorption kinetics of MB by Fe ₂ O ₃ @FCNT-H and (B) the relationship between <i>q</i> _{e,cal} and <i>k</i> _{app} under different solution pH.	18
Fig. S16. The degradation (A) and the adsorption kinetics (B) of target molecules by Fe ₂ O ₃ @FCNT-H with and without H ₂ O ₂	18
Fig. S17. The adsorption kinetics of target molecules onto Fe ₂ O ₃ @FCNT-H.....	19
Fig. S18. The change of UV-vis absorbance of MB in the presence of MO, aniline, and/or C2R as a function of reaction time.	20
Fig. S19. Effect of light irradiation and O ₂ on MB removal.....	20
Fig. S20. Fe K-edge XANES of Fe ₂ O ₃ , Fe foil, Fe ₂ O ₃ @FCNT-H, and Fe ₂ O ₃ @FCNT-H in the presence of H ₂ O ₂	21
Part S4 Supplementary Tables	22

Table S1. $^1\text{O}_2$ - mediated oxidation of various organic and inorganic compounds.....	22
Table S2. Reactions involving $\text{HO}_2^\bullet/\text{O}_2^\bullet$ in the Haber-Weiss cycle.....	23
Table S3. The chemical properties of target molecules	24
Table S4. The detection methods of organic molecules by UHPLC	25
References	26

Part S1 Supplementary Discussion

Effect of pH on $^1\text{O}_2$ generation and MB removal

In this section, we would like to discuss the effect of pH (from 2.0 - 9.0) on the MB removal in the $\text{Fe}_2\text{O}_3@\text{FCNT-H}/\text{H}_2\text{O}_2$ system from three perspectives, *i.e.*, the reaction between $^1\text{O}_2$ and MB, the generation of $^1\text{O}_2$, the adsorption of MB.

Reaction between $^1\text{O}_2$ and MB. It is accepted that pH would affect a chemical reaction through the protonation/deprotonation of the reactants (S1). In the case of reaction between $^1\text{O}_2$ and MB, as the status of MB is constant in the pH range of 2.0 - 9.0 (S2), we exclude the pH factor.

$^1\text{O}_2$ generation. Based on the Haber-Weiss cycle, $^1\text{O}_2$ should be generated from $\text{HO}_2^\bullet/\text{O}_2^{\bullet-}$ (S3). We are convinced by two facts, one is MB could not be degraded by $\text{HO}_2^\bullet/\text{O}_2^{\bullet-}$, which is generated in xanthine-xanthine oxidase system (*SI Appendix*, Fig. S12), the other is the addition of a typical $\text{HO}_2^\bullet/\text{O}_2^{\bullet-}$ quenching molecule, superoxide dismutase (SOD), effectively suppressed MB degradation in our $\text{Fe}_2\text{O}_3@\text{FCNT-H}/\text{H}_2\text{O}_2$ system (*SI Appendix*, Fig. S13). These two facts provide solid evidence for the $^1\text{O}_2$ generation through $\text{HO}_2^\bullet/\text{O}_2^{\bullet-}$ as the intermediate. We then investigated the generation of $\text{HO}_2^\bullet/\text{O}_2^{\bullet-}$ and $^1\text{O}_2$ under different pH conditions. The normalised double integration of the ESR spectra was used to semi-quantify both $\text{HO}_2^\bullet/\text{O}_2^{\bullet-}$ and $^1\text{O}_2$ (S4-6). *SI Appendix*, Fig. S14A shows that the amount of $\text{HO}_2^\bullet/\text{O}_2^{\bullet-}$ increases dramatically from pH 2.0 to 3.0, and then remains almost stable from pH 3.0 to 9.0. *SI Appendix*, Fig. S14B shows that the amount of $^1\text{O}_2$ increases steadily from pH 2.0 to 6.0, and then remains stable from pH 6.0 to 9.0. Based on the pKa value of $\text{HO}_2^\bullet/\text{O}_2^{\bullet-}$ (4.8), we could calculate the amount of $\text{O}_2^{\bullet-}$ at various pH values, and plotted them versus the amount of $^1\text{O}_2$ in *SI Appendix*, Fig. S14C, showing a linear relationship. Meanwhile, the amount of $^1\text{O}_2$ is linearly proportional to the MB degradation constant k_{app} , as shown in *SI Appendix*, Fig. S14D. Consequently, we propose that pH affects the $^1\text{O}_2$ generation for MB degradation through affecting the protonation/ deprotonation status of $\text{HO}_2^\bullet/\text{O}_2^{\bullet-}$.

Adsorption of MB. *SI Appendix*, Fig. S15A shows the improved MB adsorption as the increase of pH value for $\text{Fe}_2\text{O}_3@\text{FCNT-H}$, with the maximum adsorption capacity at equilibrium ($q_{\text{e,cal}}$) positively correlated with MB degradation k_{app} (*SI Appendix*, Fig. S15B). Since we have shown an adsorption-dependent removal feature of $\text{Fe}_2\text{O}_3@\text{FCNT-H}$ in Fig. 6A in the main text, we reckon that pH could affect the MB

adsorption, and thus affect the MB removal.

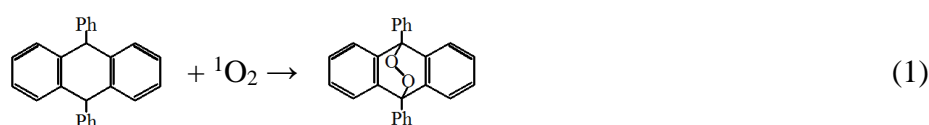
Thus, for the $\text{Fe}_2\text{O}_3@\text{FCNT-H}/\text{H}_2\text{O}_2$ system, pH plays a crucial role in the MB removal through affecting the $^1\text{O}_2$ generation as well as the MB adsorption.

Part S2 Supplementary Experimental Section

Text S1 The intermediate products detection by UHPLC/MS

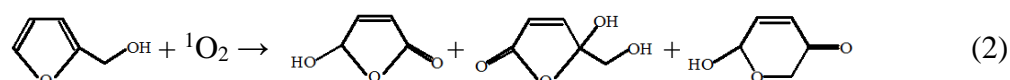
An UHPLC/MS with an electron spray ionization (ESI) source was employed to identify the intermediate products.

(i) The intermediate products from the oxidation of DPA



10 μM DPA was oxidized in the $\text{Fe}_2\text{O}_3@\text{FCNT-H}/\text{H}_2\text{O}_2$ system. The reaction was conducted in a 10-mL Teflon-line screw-cap glass vial under magnetic stirring at 293.2 ± 0.3 K. 50 mM ACN was added to ensure the dissolution of DPA. The reaction aliquot was withdrawn at the end of the reaction (60 min) and filtered through a PTFE membrane (0.22 μm) to remove the solid catalysts for analysis. UHPLC/MS with an ESI source in the positive ionization mode was used for analysis. An Agilent Eclipse plus C18 column (4.6 \times 100 mm, 3.5 μm particle size) was used for UHPLC separation. The flow rate was set at 0.2 $\text{mL}\cdot\text{min}^{-1}$. To eliminate the possible contamination of mass spectrometer by the oxidants and other impurities in the samples, the UHPLC effluent in the first 2 minutes was diverted to the waste through a switching valve between the UHPLC column outlet and the mass detector inlet. The gradient mobile phase consisted of ACN (A) and Milli-Q water (B), which increased linearly from 65/35 to 95/5 (v/v, A/B) in first 25 min and held for 10 min, and then returned to 65/35 in 0.5 min, and kept for 5 min for re-equilibration. The MS parameters were optimized and set as follows: scan type, full mass; resolution, 35000; sheath gas flow rate, 20 arbitrary units; aux gas flow rate, 10 arbitrary units; spray voltage, 3000 V; capillary temperature, 593.2 K.

(ii) The intermediate products from the oxidation of FFA



A relatively high concentration of FFA (1 or 5 mM) was oxidized in the

Fe₂O₃@FCNT-H/H₂O₂ system. The reaction was conducted in a 10-mL Teflon-line screw-cap glass vial under magnetic stirring at 293.2 ± 0.3 K. The reaction aliquots were withdrawn after 60 min and only 2.0% and 3.4% of FFA were degraded, respectively. The samples were filtered through a hydrophilic polyether sulfone (PES) membrane (0.22 μm) to remove the solid catalysts for subsequent analysis. The UHPLC/MS with an ESI source in the negative ionization mode was employed for analysis. An Agilent Eclipse plus C18 column (4.6 × 100 mm, 3.5 μm particle size) was used for UHPLC separation. The flow rate was set at 0.2 mL·min⁻¹. To eliminate the possible contamination of mass spectrometer by the oxidants and other impurities in the samples, the UHPLC effluent in the first 2 minutes was diverted to the waste through a switching valve between the UHPLC column outlet and the mass detector inlet. The gradient mobile phase consisted of MeOH (A) and Milli-Q water (B), which increased linearly from 5/95 to 20/80 (v/v, A/B) in first 20 min and hold for 15 min, and then returned to 5/95 in 0.5 min, and kept for 5 min for re-equilibration. The MS parameters were optimized and set as follows: scan type, full mass; resolution, 35000; sheath gas flow rate, 35 arbitrary units; aux gas flow rate, 10 arbitrary units; spray voltage, 2500 V; capillary temperature, 573.15 K.

Text S2 Calculation of the concentration of products

The standard sample of the products (*i.e.*, C₅H₆O₄, C₄H₄O₃, and C₅H₆O₃) from the oxidation of FFA by ¹O₂ cannot be readily available. Thus, the calculation of their concentrations from the UHPLC peak area was conducted on the basis of the molar adsorption coefficients using FFA as a reference at 219 nm, as reported by Richard et al (S7). The molar adsorption coefficient of C₅H₆O₄, C₄H₄O₃, C₅H₆O₃, and FFA was 1320 ± 40, 2000, 7500 ± 200, and 8100 ± 60 M⁻¹·cm⁻¹, respectively (S8). Thus, the concentration of C₅H₆O₄, C₄H₄O₃, and C₅H₆O₃ was calculated on the basis of the Lambert-Beer law:

$$A = \varepsilon bc \quad (3)$$

Where A is the absorbance (here is the peak area), ε represents the molar adsorption coefficient, b is the optical depth through the sample, c is the concentration of the sample.

$$\frac{A_{product}}{A_{FFA}} = \frac{\varepsilon_{product}}{\varepsilon_{FFA}} \times \frac{c_{product}}{c_{FFA}} \quad (4)$$

$$c_{product} = \frac{A_{product}}{A_{FFA}} \times \frac{\varepsilon_{FFA}}{\varepsilon_{product}} \times c_{FFA} \quad (5)$$

We obtained c_{FFA} / A_{FFA} of 1/24330 from the inverse slope of the standard calibration of FFA. Thus, the above equation can be further simplified:

$$c_{product} = \frac{\varepsilon_{FFA} \times A_{product}}{24330 \times \varepsilon_{product}} \quad (6)$$

According to eq 6, the concentration of the products can be calculated.

Text S3 Chemicals and materials

Multi-walled carbon nanotubes (MWCNTs, I.D. 5-10 nm, O.D. 10-20 nm, length 10-30 μm) were purchased from Chengdu Organic Chemicals Co., Ltd. (China) with purity of $\geq 98\%$. Mesoporous silica (SBA-15, I.D. 6-11 nm), and graphene oxide (GO) were obtained from Nanjing XFNANO Materials Tech Co., Ltd. (China). Aniline, dimethyl sulfoxide (DMSO), superoxide dismutase (SOD), furfuryl alcohol (FFA), tertiary butanol (TBA), and 1,10-phenanthroline of analytical grade or better were obtained from Shanghai Aladdin Biochemical Technology Co., Ltd. (China). $\text{Fe}(\text{NO}_3)_3 \cdot 9\text{H}_2\text{O}$, HNO_3 , HCl , H_2O_2 (in water), acetone, methylene blue (MB), methyl violet (MV), crystal violet (CV), chrysoidine, malachite green oxalate (MGO), methyl orange (MO), and chromotrope 2R (C2R) were received from Sinopharm Chemical Reagent Co., Ltd. (China) and used without further purification. Their basic properties are shown in *SI Appendix*, Table S3. 4-Chlorophenol (4-CP), 2,2,6,6-tetramethyl-4-piperidinol (TEMP), 5,5-dimethyl-1-pyrrolin-*N*-oxide (DMPO), and 9,10-diphenylanthracene (DPA) of ACS reagents were purchased from Sigma-Aldrich (U.S.A). Methanol (MeOH) and acetonitrile (ACN) of HPLC grade were purchased from Merck (Germany). All of the stock solutions were prepared in ultrapure water (18.25 $\text{M}\Omega\cdot\text{cm}$) except insoluble DPA. 1 mM DPA stock solution was prepared using ACN as the solvent.

Text S4 The transfer of XRD patterns

The crystalline structures of the catalysts were determined by X-ray diffraction analysis (XRD, D-MAX Rapid-II, Rigaku, Japan) using $\text{Mo K}\alpha$ radiation ($\lambda = 0.7093 \text{ \AA}$). For better analysis and comparison with the data from XRD in $\text{Cu K}\alpha$ radiation, the obtained XRD spectra were transferred according to the Bragg equation as follows :

$$2d \sin \theta = n\lambda \quad (7)$$

Where d is the interplanar crystal spacing, \AA ; θ is the angle between X ray and the crystal surface; n represents diffraction series; λ is the wavelength of X ray. For a

given sample, d-spacing will not change regardless of the X ray species and thus the transformation of θ in different model can be achieved as follows:

$$\frac{\sin \theta_{Cu}}{\sin \theta_{Mo}} = \frac{\lambda_{Cu}}{\lambda_{Mo}} \quad (8)$$

$$\theta_{Mo} = \arcsin\left(\frac{\lambda_{Cu}}{\lambda_{Mo}} \times \sin \theta_{Mo}\right) \quad (9)$$

Text S5 Evaluating the stability and reusability of Fe₂O₃@FCNT-H

For the consecutive MB addition runs without regeneration, the degradation experiment was conducted in a 500-mL conical flask. The reaction was initiated by simultaneous addition of $4.0 \times 10^{-2} \text{ g}\cdot\text{L}^{-1}$ catalyst suspension and 50 mM H₂O₂ into the solution containing 10 μM MB. The reaction aliquots of 4 mL were periodically sampled by pipette and filtered through a membrane (0.22 μm) to remove the solid catalysts for MB analysis. After 60-min reaction, MB was completely degraded, and 10 μM MB was added again. For the regeneration experiment, to avoid the loss of catalysts in the cyclic runs, a large number of catalysts were prepared in an amplifying reactor. Specially, 0.14 g Fe₂O₃@FCNT-H was divided equally into two 1.75 L solutions containing 10 μM MB. The reaction was initiated by adding 50 mM H₂O₂. After 60-min reaction, the catalysts were collected by suction filtration, followed by rinsing with ethanol (EtOH) and ultrapure water in sequence for five times, the catalysts were lyophilized. The obtained solids were denoted as Fe₂O₃@FCNT-H-2nd, and we got Fe₂O₃@FCNT-H-3rd following the same procedure mentioned above. For each run, 10 mg Fe₂O₃@FCNT-H-x (x = 2nd, 3rd) was weighed by micro-balance (XP56, Mettler Toledo, Switzerland) and used for the reaction conducted in a 250 mL conical flask, where the MB solution was sampled and analyzed.

Text S6 The operation methods for reactive intermediates analysis by ESR

Qualitative analysis. The reactions were carried out in 1 mL centrifuge tubes. $1.5 \times 10^{-2} \text{ g}\cdot\text{L}^{-1}$ catalyst (*i.e.*, Fe₂O₃, Fe₂O₃/FCNT-L, or Fe₂O₃@FCNT-H), 50 mM H₂O₂ were added orderly to 160 μL solution containing 50 mM DMPO/ TEMP to made up the volume to 200 μL . After ca. 5 min, the solutions were sucked to capillary tubes and determined on an ESR A300 spectrometer.

Semi-quantitative analysis. We conducted normalised double integration of the obtained ESR spectra to semi-quantify the concentration of the generated HO₂[•]/O₂^{•-} and ¹O₂ on WINEPR Processing system (S4-6). The integral intervals were set as

3455 - 3508 G for the DMPO-OOH signal and 3457 - 3505 G for the TMPN signal. As for $\text{HO}_2^\bullet/\text{O}_2^{\bullet-}$, MeOH and water (20:1, v:v) was mixed and adjusted the solution pH to 2.0 - 9.0 by 0.01 M HCl and 0.01 M NaOH in advance. In the detection process, 50 mM DMPO, $1.5 \times 10^{-2} \text{ g}\cdot\text{L}^{-1}$ $\text{Fe}_2\text{O}_3@\text{FCNT-H}$, and 50 mM H_2O_2 were added orderly to 300 μL solution with different pH. The DMPO-OOH signal was detected after 60 min of reaction. As for $^1\text{O}_2$ production, the pH of 100 mM TEMP solution is 10.1 and thus the solution pH is adjusted to ca. 4.8 in advance. In the detection process, 10 mM TEMP, $1.5 \times 10^{-2} \text{ g}\cdot\text{L}^{-1}$ $\text{Fe}_2\text{O}_3@\text{FCNT-H}$, and 50 mM H_2O_2 were added orderly to 300 μL solution with different pH. The TMPN signal was detected at 60 min.

Part S3 Supplementary Figures

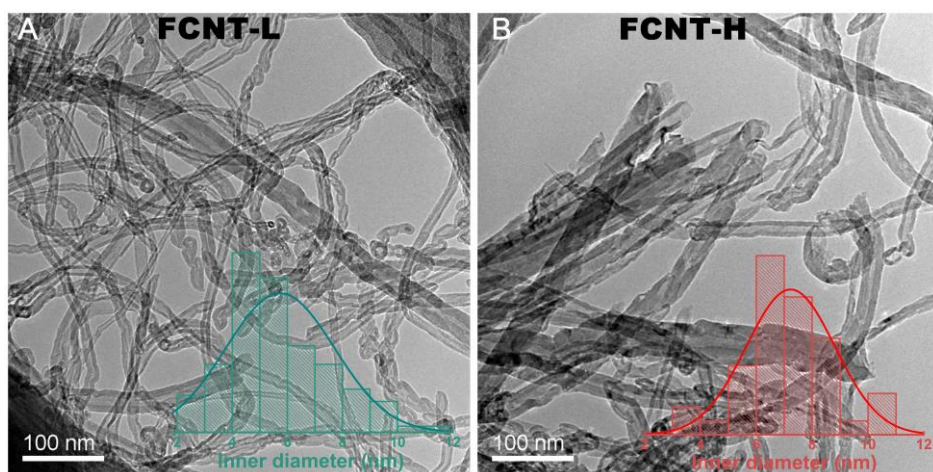


Fig. S1. TEM images of (A) FCNT-L and (B) FCNT-H. The insets are inner diameter distribution of both CNTs.

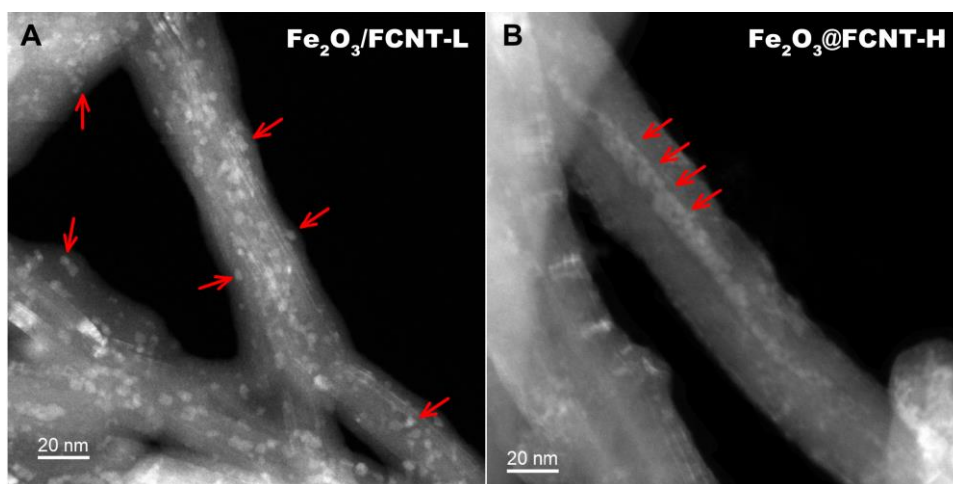


Fig. S2. STEM-HAADF images of (A) Fe₂O₃/FCNT-L and (B) Fe₂O₃@FCNT-H.

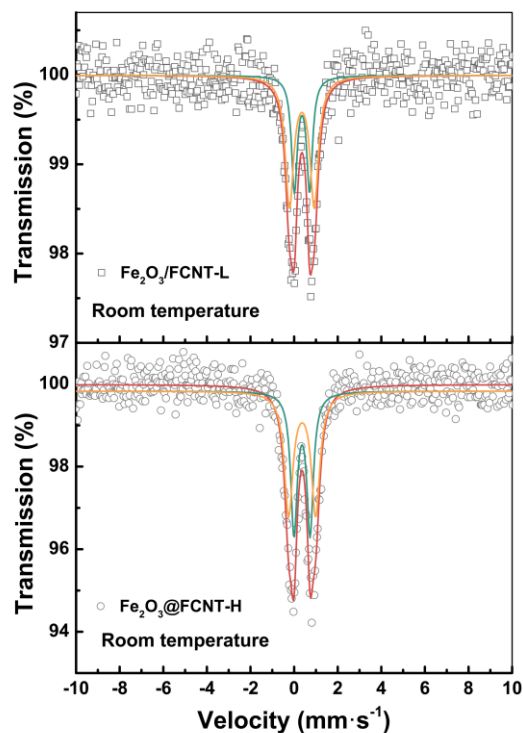


Fig. S3. ^{57}Fe Mössbauer spectra of both $\text{Fe}_2\text{O}_3/\text{FCNT-L}$ and $\text{Fe}_2\text{O}_3@\text{FCNT-H}$ at room temperature. Both samples show the central doublets in the spectra which may due to the ultrafine nanoparticles as verified by TEM images. The spectra confirm the sole presence of Fe^{3+} species by the uniform isomer shift (IS) of $\text{ca.}0.36 \text{ mm}\cdot\text{s}^{-1}$ relative to alpha-iron (S9-12). Combined with the quadrupole splitting (QS) of the fitted doublets in the range of $0.69 \text{ mm}\cdot\text{s}^{-1} - 1.23 \text{ mm}\cdot\text{s}^{-1}$, we can confirm the existence of FeO_6 -type octahedral coordination for both samples (S9-11).

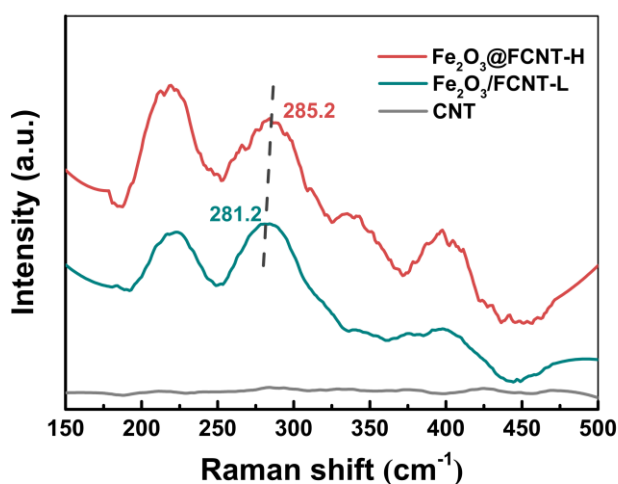


Fig. S4. Raman spectra of the catalysts.

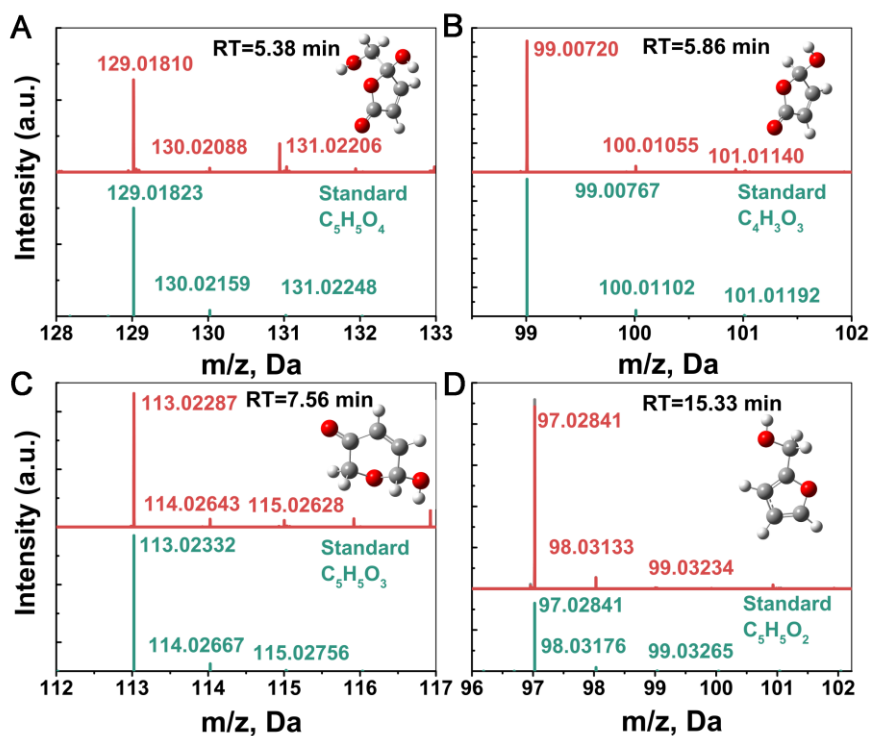


Fig. S5. The molecular mass spectra of the detected (A) $C_5H_6O_4$, (B) $C_4H_4O_3$, (C) $C_5H_6O_3$, and (D) FFA in negative ionization mode by UHPLC/MS.

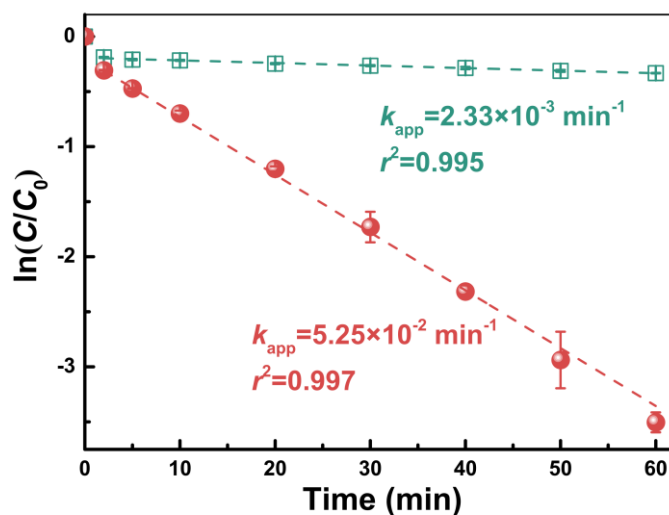


Fig. S6. The kinetics of MB degradation in both $Fe_2O_3@FCNT-H/H_2O_2$ system and $Fe_2O_3/FCNT-L/H_2O_2$ system. Reaction conditions: pH = 5.0, T = 293.2 K, $[Fe_2O_3@FCNT-H] = [Fe_2O_3/FCNT-L] = 1.5 \times 10^{-2} \text{ g} \cdot \text{L}^{-1}$, $[MB] = 10 \text{ } \mu\text{M}$, $[H_2O_2] = 50 \text{ mM}$.

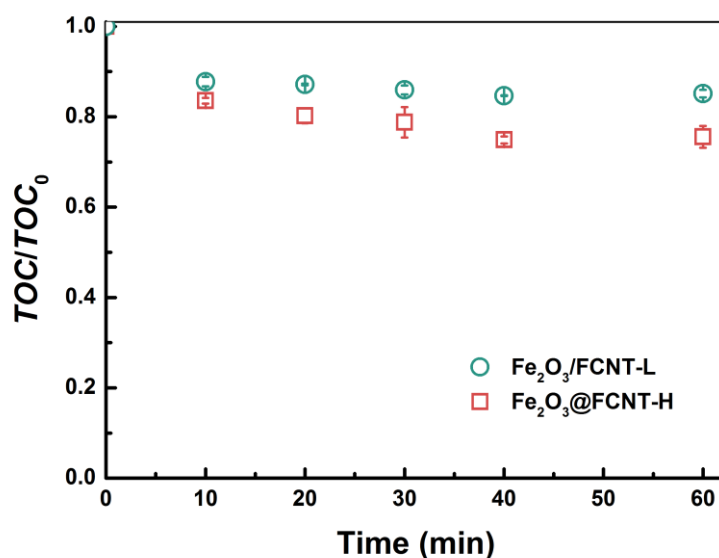


Fig. S7. TOC removal during MB degradation in both Fe₂O₃@FCNT-H/H₂O₂ system and Fe₂O₃/FCNT-L/H₂O₂ system. Reaction conditions: pH = 5.0, T = 293.2 K, [Fe₂O₃@FCNT-H] = [Fe₂O₃/FCNT-L] = $1.5 \times 10^{-2} \text{ g}\cdot\text{L}^{-1}$, [MB] = 10 μM , [H₂O₂] = 50 mM.

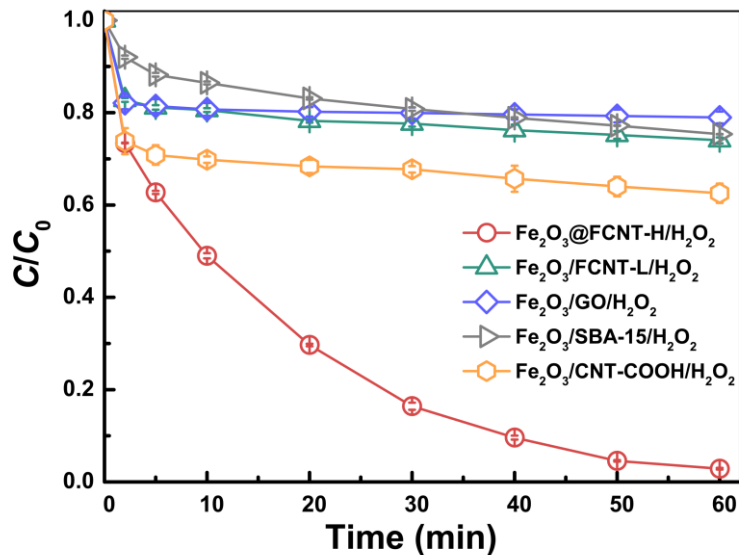


Fig. S8. The degradation of MB in the different systems. Reaction conditions: pH = 5.0, T = 293.2 K, [catalysts] = $1.5 \times 10^{-2} \text{ g}\cdot\text{L}^{-1}$, [MB] = 10 μM , [H₂O₂] = 50 mM. The Fe loading is 2 wt. % for all the catalysts.

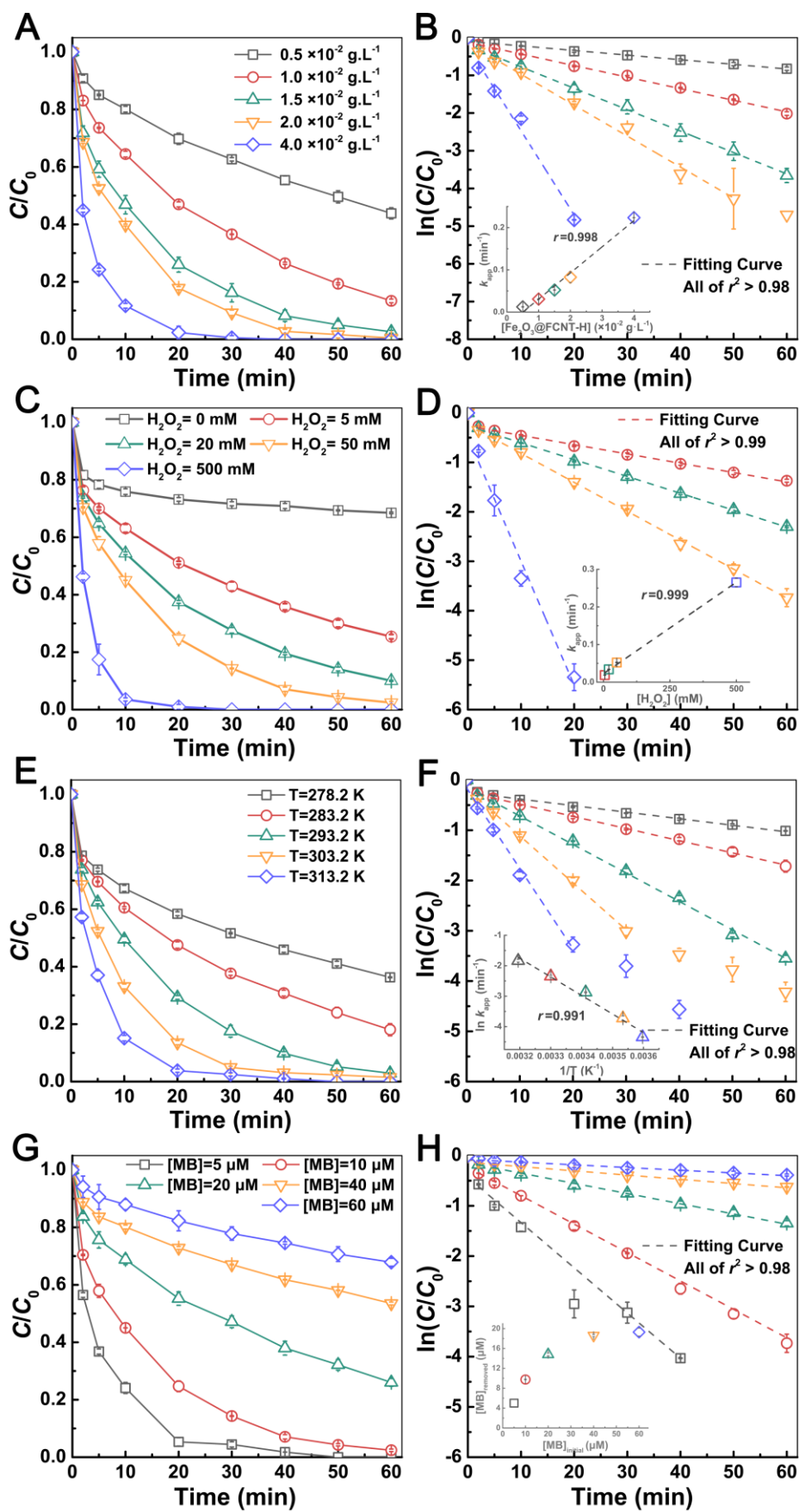


Fig. S9. MB removal under different conditions. The effect of (A-B) catalyst dosage, (C-D) H_2O_2

concentration, (*E-F*) reaction temperature, and (*G-H*) initial MB concentration on MB degradation and corresponding degradation kinetics in Fe₂O₃@FCNT-H/H₂O₂ system. The insets show the relationship between (*B*) catalyst dosage, (*D*) H₂O₂ concentration, (*F*) reaction temperature and *k*_{app} of MB degradation. The inset in (*H*) shows the relationship between the concentration of removed MB and initial MB concentration. Experimental conditions: pH = 5.0, T = 278.2 - 313.2 K, [Fe₂O₃@FCNT-H] = 0.5 - 4.0 × 10⁻² g·L⁻¹, [MB] = 5 - 60 μM, [H₂O₂] = 0 - 500 mM. These results show that the increase of catalyst dosage (*A*) and H₂O₂ concentration (*B*) could remarkably increase ¹O₂ production and subsequently enhance MB degradation. The linear correlations between the catalyst dosage/ H₂O₂ concentration and *k*_{app} values (*B* and *D*, *r* > 0.99) suggest the direct generation of ¹O₂ from H₂O₂ activation by Fe₂O₃@FCNT-H. Results in (*E-F*) show that the increase of reaction temperature also effectively accelerate the MB degradation and the apparent activation energy could be calculated based on Arrhenius equation to be 50.7 kJ·mol⁻¹. As the increase of initial MB concentration, the *k*_{app} value decreases, however, the total removed quantity increases. Results in the inset of (*H*) indicate the amount of ¹O₂ generated by the Fe₂O₃@FCNT-H/H₂O₂ system under the present condition could degrade ca. 20 μM MB within 60 min.

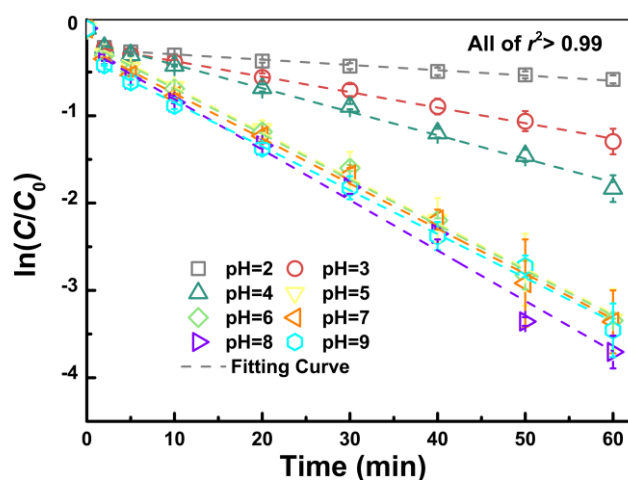


Fig. S10. The MB degradation kinetics under different solution pH in Fe₂O₃@FCNT-H/H₂O₂ system. Reaction conditions: pH = 3.0 - 9.0, T = 293.2 K, [catalysts] = 1.5 × 10⁻² g·L⁻¹, [MB] = 10 μM, [H₂O₂] = 50 mM.

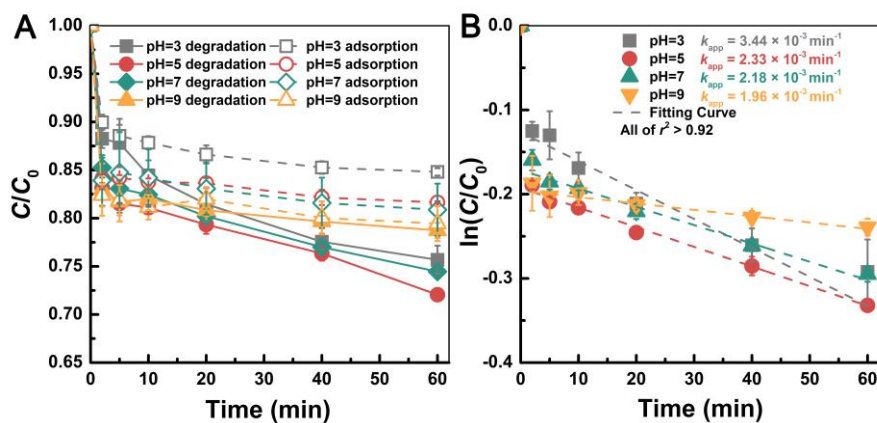


Fig. S11. The effect of solution pH on (A) MB removal by $\text{Fe}_2\text{O}_3/\text{FCNT-L}$ with/without H_2O_2 and (B) degradation kinetics. Reaction conditions: pH = 3.0 - 9.0, $T = 293.2 \text{ K}$, $[\text{Fe}_2\text{O}_3/\text{FCNT-L}] = 1.5 \times 10^{-2} \text{ g}\cdot\text{L}^{-1}$, $[\text{MB}] = 10 \mu\text{M}$, $[\text{H}_2\text{O}_2] = 50 \text{ mM}$.

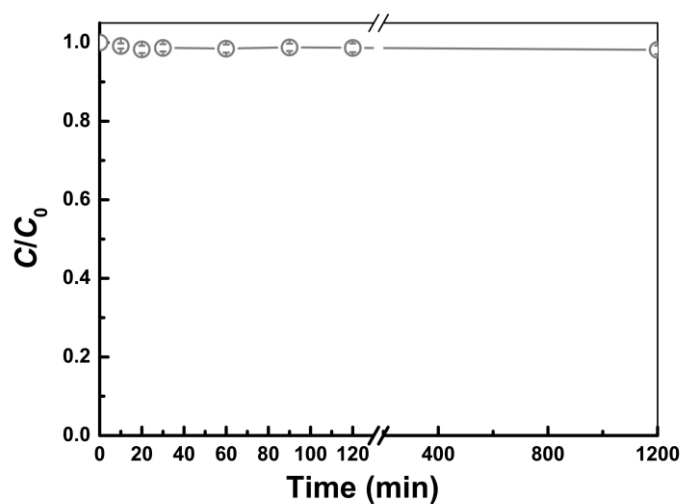


Fig. S12. MB removal in xanthine-xanthine oxidase system. Reaction conditions: pH = 7.8, $T = 293.2 \text{ K}$, [phosphate buffer] = 10 mM, $[\text{MB}] = 10 \mu\text{M}$, [xanthine] = 1 mM, [xanthine oxidase] = 125 $\text{mU}\cdot\text{mL}^{-1}$.

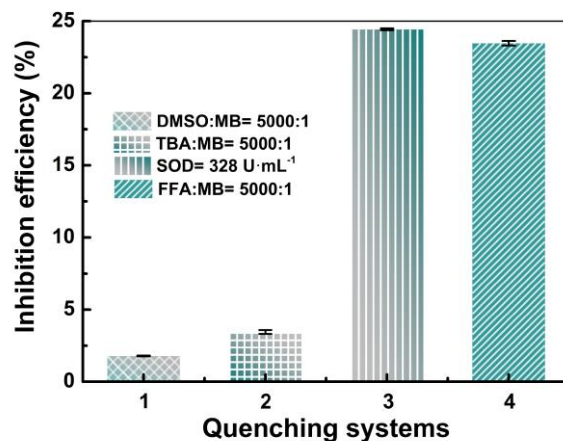


Fig. S13. The inhibition efficiency of the catalytic activity of Fe₂O₃@FCNT-H using different quenching molecules. Reaction conditions: pH = 5.0, T = 293.2 K, [Fe₂O₃@FCNT-H] = 1.5 × 10⁻² g·L⁻¹, [MB] = 10 μM, [H₂O₂] = 50 mM, [TBA] = [FFA] = [DMSO] = 50 mM, [SOD] = 328 U·mL⁻¹.

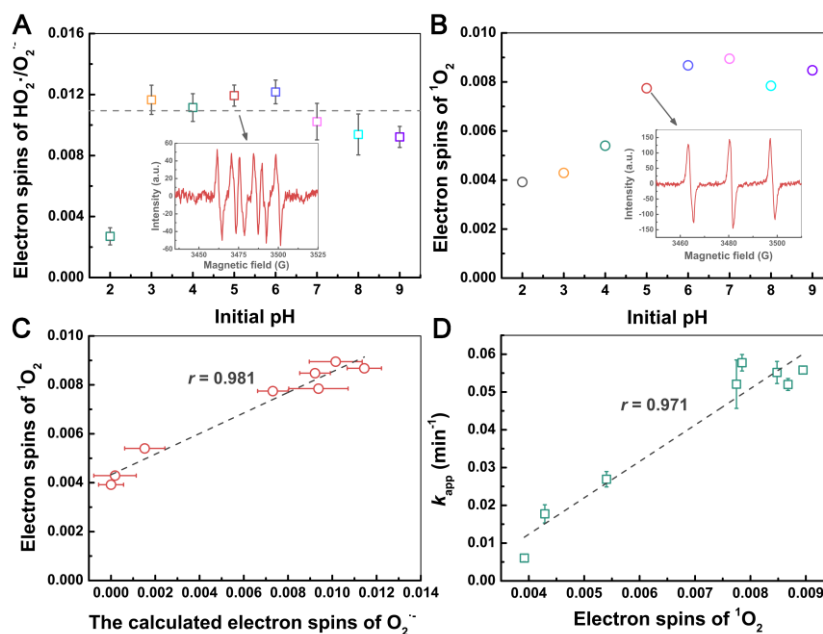


Fig. S14. The effect of pH on HO₂•/O₂•⁻ and ¹O₂ generation. The effect of pH on (A) electron spins of HO₂•/O₂•⁻ trapped by DMPO and (B) electron spins of ¹O₂ trapped by TEMP in Fe₂O₃@FCNT-H/H₂O₂ system. (C) The relationship between the calculated electron spins of O₂•⁻ and electron spins of ¹O₂. (D) The relationship between electron spins of ¹O₂ and k_{app} value. Reaction conditions: pH = 2.0 - 9.0, T = 293.2 K, [Fe₂O₃@FCNT-H] = 1.5 × 10⁻² g·L⁻¹, [H₂O₂] = 50 mM, [DMPO] = 50 mM for (A) and [TEMP] = 50 mM for (B).

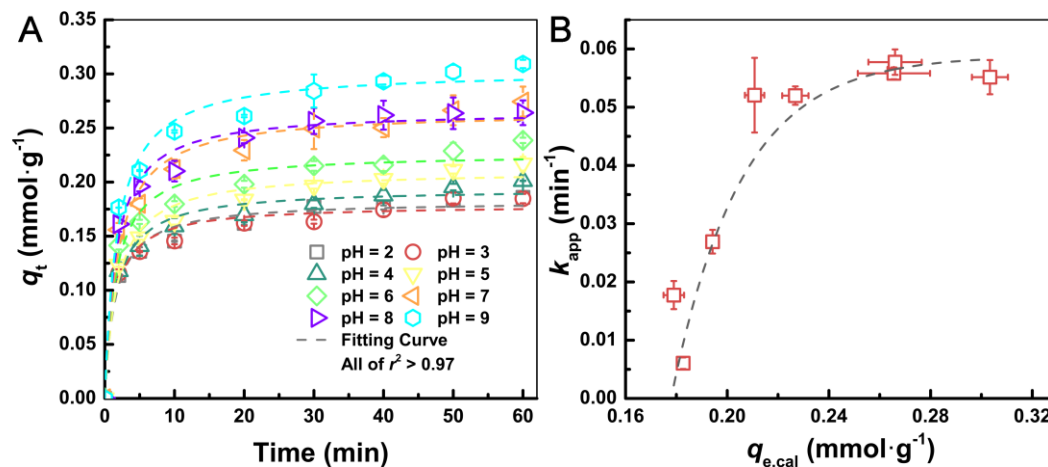


Fig. S15. (A) The adsorption kinetics of MB by Fe₂O₃@FCNT-H and (B) the relationship between $q_{e,cal}$ and k_{app} under different solution pH. Reaction conditions: pH = 2.0 - 9.0, T = 293.2 K, [Fe₂O₃@FCNT-H] = 1.5×10^{-2} g·L⁻¹, [MB] = 10 μM.

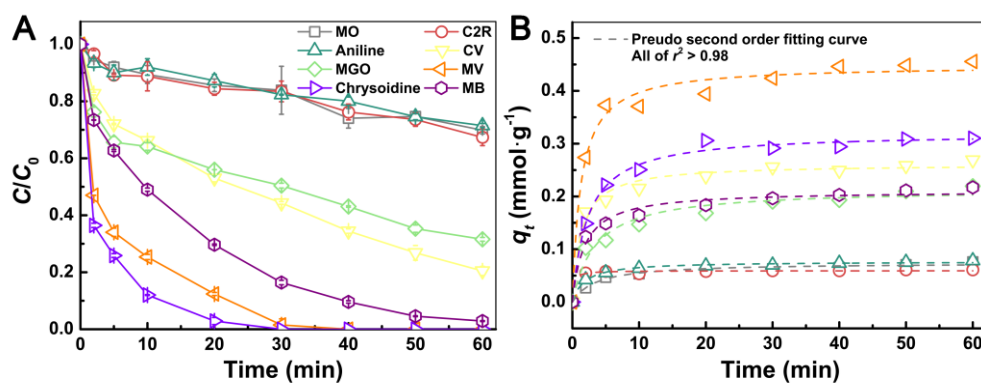


Fig. S16. The degradation (A) and the adsorption kinetics (B) of target molecules by Fe₂O₃@FCNT-H with and without H₂O₂. Reaction conditions: pH = 5.0, T = 293.2 K, [Fe₂O₃@FCNT-H] = 1.5×10^{-2} g·L⁻¹, [target molecules] = 10 μM, [H₂O₂] = 0/50 mM.

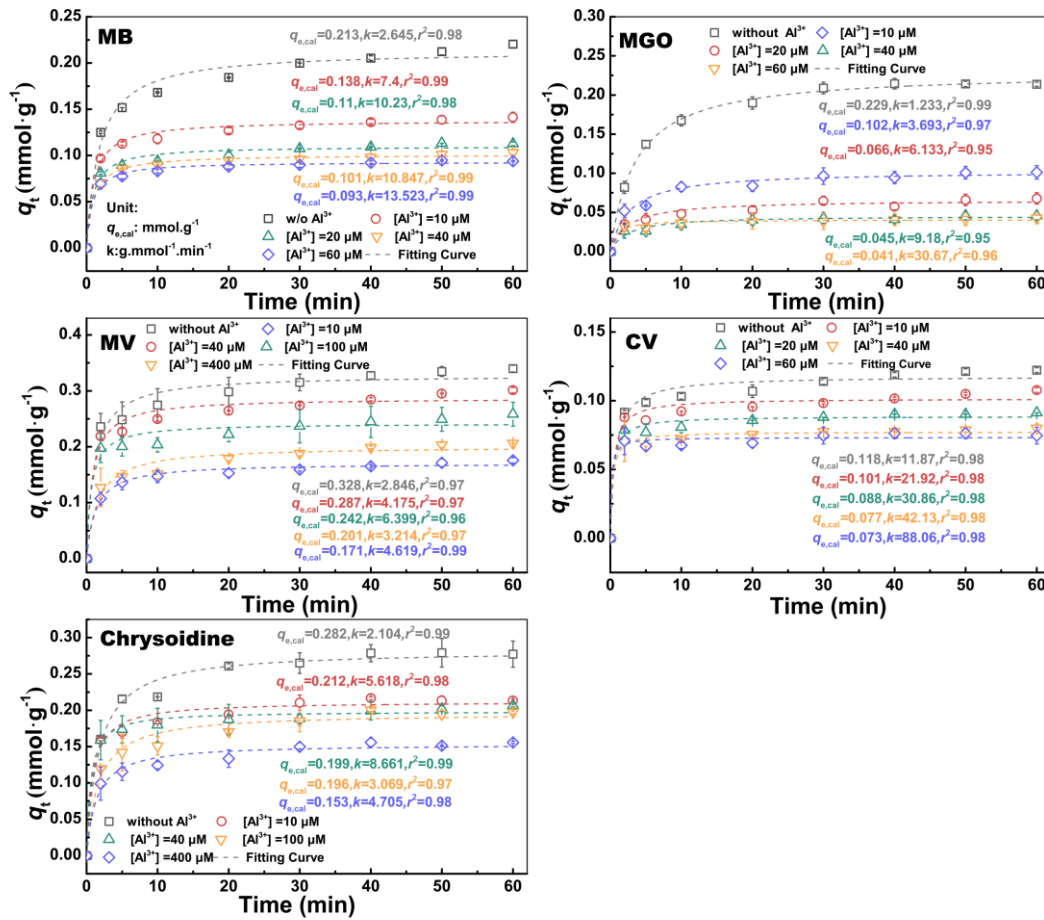


Fig. S17. The adsorption kinetics of target molecules onto $\text{Fe}_2\text{O}_3@\text{FCNT-H}$. Reaction conditions: $\text{pH} = 5.0$, $T = 293.2 \text{ K}$, $[\text{Fe}_2\text{O}_3@\text{FCNT-H}] = 1.5 \times 10^{-2} \text{ g}\cdot\text{L}^{-1}$, $[\text{Al}^{3+}] = 0.1 - 1 \text{ mM}$, $[\text{target molecules}] = 10 \mu\text{M}$.

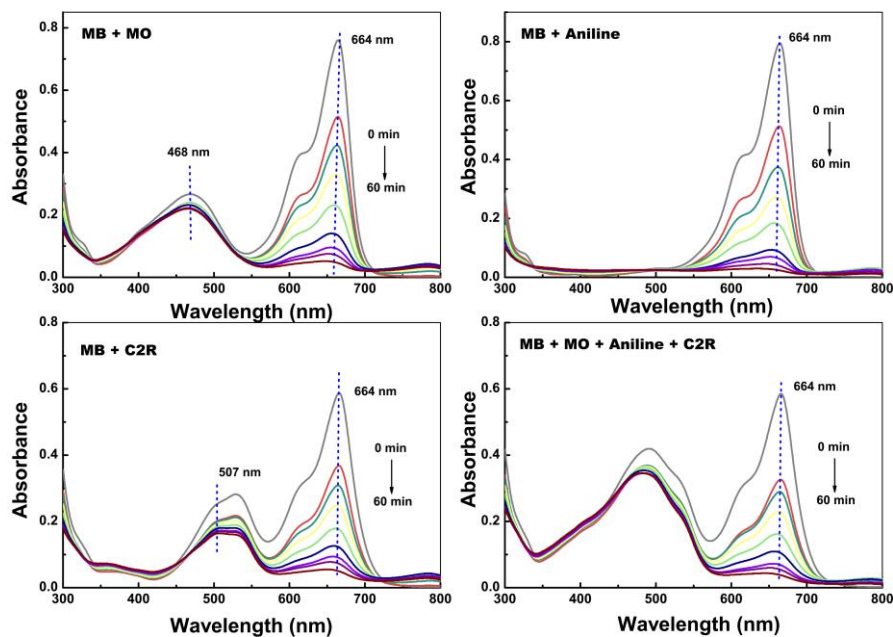


Fig. S18. The change of UV-vis absorbance of MB in the presence of MO, aniline, and/or C2R as a function of reaction time. Reaction conditions: pH = 5.0, T = 293.2 K, $[\text{Fe}_2\text{O}_3@\text{FCNT-H}] = 1.5 \times 10^{-2} \text{ g}\cdot\text{L}^{-1}$, [target molecules] = 10 μM , $[\text{H}_2\text{O}_2] = 50 \text{ mM}$.

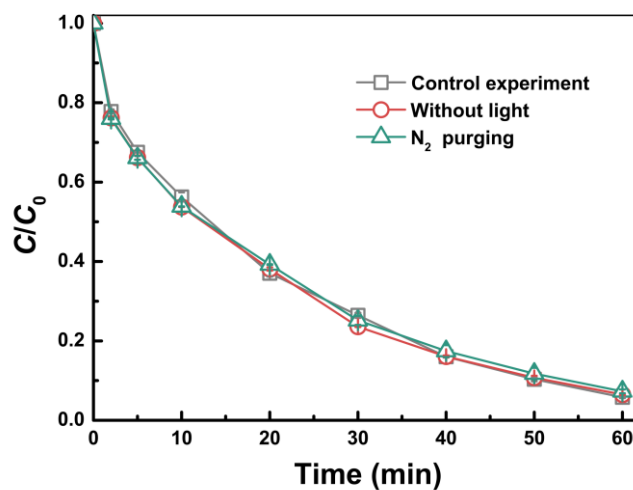


Fig. S19. Effect of light irradiation and O_2 on MB removal. Reaction conditions: pH = 5.0, T = 293.2 K, $[\text{Fe}_2\text{O}_3@\text{FCNT-H}] = 1.5 \times 10^{-2} \text{ g}\cdot\text{L}^{-1}$, $[\text{MB}] = 10 \mu\text{M}$, $[\text{H}_2\text{O}_2] = 50 \text{ mM}$.

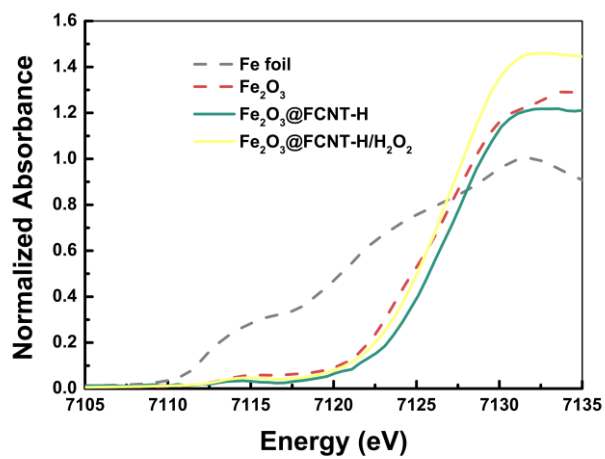


Fig. S20. Fe K-edge XANES of Fe₂O₃, Fe foil, Fe₂O₃@FCNT-H, and Fe₂O₃@FCNT-H in the presence of H₂O₂.

Part S4 Supplementary Tables

Table S1. $^1\text{O}_2$ - mediated oxidation of various organic and inorganic compounds

Classification	Compound*	Solvent	pH	$k ^1\text{O}_2$ ($\text{M}^{-1}\cdot\text{s}^{-1}$) [§]	Ref.
Dyes	MB	H ₂ O	5.9	3.0×10^8	(S13)
	eosin	ACN	-	5.0×10^7	(S14)
	rose bengal	ACN	-	7.2×10^7	(S14)
	leucomalachite green	toluene	-	2.0×10^8	(S15)
	phenol [†]	H ₂ O	≤ 8.0	$2.6 \pm 4.0 \times 10^6$	(S1)
	4-chlorophenol [†]	H ₂ O	≤ 7.4	$6.0 \pm 3.6 \times 10^6$	(S1)
	2-nitrophenol [†]	H ₂ O	≤ 5.2	$1.3 \pm 1.1 \times 10^6$	(S1)
	4-methylphenol [†]	H ₂ O	≤ 8.3	$9.6 \pm 2.8 \times 10^6$	(S1)
Aromatic compounds	1,3-benzenediol	EtOH	-	7.9×10^5	(S16)
	1,4-benzenediol	pyridine	-	$2.5\text{-}4.0 \times 10^7$	(S16)
	2,6-di- <i>t</i> -butylphenol	MeOH	-	1.0×10^6	(S17)
	2,4,6-triphenylphenol	MeOH	-	2.5×10^8	(S17)
	1,2,4-trimethoxybenzene	MeOH	-	1.8×10^7	(S17)
	2,4,6-trichlorophenol [†]	H ₂ O	≤ 7.4	$1.7 \pm 0.7 \times 10^7$	(S1)
	aniline	MeOH	-	2.0×10^9	(S18)
	naphthalene	1-BuOH [‡]	-	5.2×10^8	(S15)
	9,10-diphenylanthracene	benzene	-	1.2×10^6	(S19)
	histidine	H ₂ O	8.5	6.6×10^7	(S20)
Amine acids	methionine	H ₂ O	8.5	$2.2 \pm 0.7 \times 10^7$	(S20)
	tyrosine	H ₂ O	8.5	0.9×10^7	(S20)
	tryptophan	H ₂ O	8.5	1.8×10^8	(S20)
	furfuryl alcohol	H ₂ O	5.0-12.0	1.2×10^8	(S21)
Heterocyclic compounds	2,5-dimethylfuran	H ₂ O	7.0	8.2×10^8	(S15)
	cyanohemoglobin	H ₂ O	7.0	1.2×10^9	(S15)
	porphyrin	CHCl ₃	-	4.2×10^8	(S15)
	cytochrome C	H ₂ O	7.4	1.4×10^8	(S15)
	β -carotene	MeOH	-	9.3×10^8	(S15)
	crocetin	H ₂ O	7.8	5.7×10^9	(S15)
Olefins	oleic acid	ACN	-	1.6×10^5	(S15)
	1,4-dioxene	Ace [‡]	-	$2.2\text{-}3.6 \times 10^5$	(S15)
	polyisoprene	CHCl ₃	-	1.2×10^5	(S15)
Inorganic compounds	azide ion	H ₂ O	7.0	$4.5\text{-}6.4 \times 10^8$	(S15)
	iodide ion	H ₂ O	7.0	8.7×10^5	(S15)
	nitrate ion	H ₂ O	8.3	3.1×10^6	(S15)
	O ₂ ⁻	DMSO	-	1.6×10^9	(S15)

* Various compounds have been reported to be oxidized by $^1\text{O}_2$ generated from different systems. For examples, MoO_4^{2-} - exchanged layered double hydroxides could effectively catalyze H_2O_2

decomposition to produce $^1\text{O}_2$ to oxidize chemicals including 2,3-dimethyl-2-butene, olefins, and allylic alcohols, through either the ene hydroperoxidation or the [2+4] cycloaddition (S23). Pharmaceutical compounds such as cimetidine, propranolol, ranitidine, sulfamethoxazole could be effectively degraded by $^1\text{O}_2$ generated from either alkaline periodate (S24) or peroxymonosulfate activation by benzoquinone (S25). Dissolved organic matter could also be partially degraded by $^1\text{O}_2$, resulting in slower bacterial growth (S26). Apoptosis of the cancer cells was reported in the *in vitro* photodynamic therapy due to $^1\text{O}_2$ generation from ultrathin black phosphorus nanosheets under light irradiation (S27).

† Phenolate anions dominate at higher pH values above pK_a . The rate constants for the reactions between phenolate anions and $^1\text{O}_2$ are always one order of magnitude higher than those involving the undissociated phenols (S1).

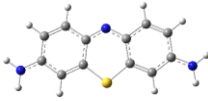
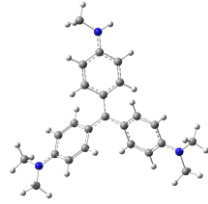
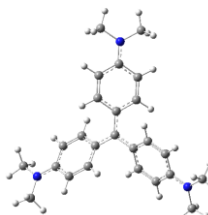
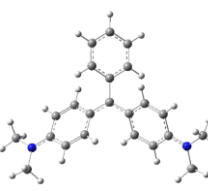
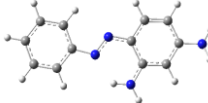
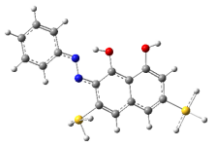
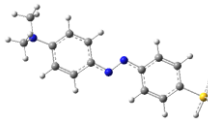
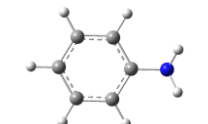
‡ 1-BuOH is the abbreviation of 1-butanol, and Ace is the abbreviation of acetone.

§ The values of rate constant are the sum of that of the chemical oxidation ($\text{A} + ^1\text{O}_2 \rightarrow \text{Products}$) and the physical quenching of $^1\text{O}_2$ by the target molecules ($\text{A} + ^1\text{O}_2 \rightarrow \text{A} + ^3\text{O}_2$).

Table S2. Reactions involving $\text{HO}_2^\bullet/\text{O}_2^{\bullet-}$ in the Haber-Weiss cycle

NO.	Reactions	k ($\text{M}^{-1}\cdot\text{s}^{-1}$)	Ref.
S1	$\text{Fe(III)} + \text{H}_2\text{O}_2 \rightarrow \text{Fe(II)} + \text{HO}_2^\bullet + \text{H}^+$	$1.0\text{-}10 \times 10^{-3}$	(S28)
S2	$\text{Fe(III)} + \text{HO}_2^\bullet \rightarrow \text{Fe(II)} + \text{H}^+ + \text{O}_2$	$<2.0 \times 10^3$	(S28)
S3	$\text{Fe(II)} + \text{HO}_2^\bullet \rightarrow \text{Fe(III)} + \text{HO}_2^-$	1.2×10^6	(S29)
S4	$\text{Fe(III)} + \text{O}_2^{\bullet-} \rightarrow \text{Fe(II)} + \text{O}_2$	1.5×10^8	(S29)
S5	$\text{Fe(II)} + \text{O}_2^{\bullet-} + 2\text{H}^+ \rightarrow \text{Fe(III)} + \text{H}_2\text{O}_2$	1.0×10^7	(S28)
S6	$\text{H}^+ + \text{O}_2^{\bullet-} \leftrightarrow \text{HO}_2^\bullet$	$k_+ 1.0 \times 10^{10}$ $k_- 1.58 \times 10^5$	(S28)
S7	$\text{HO}_2^\bullet + \text{H}_2\text{O}_2 \rightarrow \text{HO}^\bullet + \text{H}_2\text{O} + \text{O}_2$	3	(S30)
S8	$\text{HO}_2^\bullet + \text{HO}_2^\bullet \rightarrow \text{H}_2\text{O}_2 + \text{O}_2$	8.3×10^5	(S29)
S9	$\text{O}_2^{\bullet-} + \text{H}_2\text{O}_2 \rightarrow \text{HO}^\bullet + \text{OH}^- + \text{O}_2$	0.13	(S31)
S10	$\text{O}_2^{\bullet-} + \text{HO}_2^\bullet \rightarrow \text{HO}_2^- + \text{O}_2$	9.7×10^7	(S29)
S11	$\text{HO}^\bullet + \text{H}_2\text{O}_2 \rightarrow \text{HO}_2^\bullet + \text{H}_2\text{O}$	3.3×10^7	(S28)
S12	$\text{HO}^\bullet + \text{HO}_2^\bullet \rightarrow \text{H}_2\text{O} + \text{O}_2$	7.1×10^9	(S28)
S13	$\text{HO}^\bullet + \text{O}_2^{\bullet-} \rightarrow \text{OH}^- + \text{O}_2$	1.01×10^{10}	(S28)
S14	$\text{HO}^\bullet + \text{HO}^\bullet \rightarrow \text{H}_2\text{O}_2$	5.2×10^9	(S28)

Table S3. The chemical properties of target molecules

Compound	CAS No.	Structure*	Formula	Molar mass (g·mol ⁻¹)	Collision dimension [†] (Å × Å × Å)	Maximum absorption wavelength (nm)
methylene blue	7220-79-3		C ₁₆ H ₁₈ ClN ₃ S	319.9	14.3×7.6×3.8	664
methyl violet	8004-87-3		C ₂₄ H ₂₈ ClN ₃	393.96	14.5×16.4×6.1	579
crystal violet	548-62-9		C ₂₅ H ₃₀ ClN ₃	407.99	15.0×16.6×6.2	583
malachite green oxalate	569-64-2		C ₂₃ H ₂₅ ClN ₂	364.92	14.1×14.1×6.0	616
chrysoidine	532-82-1		C ₁₂ H ₁₂ N ₄ HCl	248.71	14.7×8.1×3.4	453
chromotrope 2R	4197-07-3		C ₁₆ H ₁₀ N ₂ Na ₂ O ₈ S ₂	468.37	17.9×10.0×5.8	507
methyl orange	547-58-0		C ₁₄ H ₁₄ N ₃ NaO ₃ S	327.33	19.4×5.4×7.4	464
aniline	62-53-3		C ₆ H ₇ N	93.13	8.4×7.0×3.4	263

*The geometries of the selected contaminants were optimized in the gas phase using the Gaussian 16 software package (Gaussian, Inc.) using hybrid density functional

theory (DFT), B3LYP and the 6-311G basis set. † The collision dimension estimation was carried out by Chemcraft based on the optimized geometries.

Table S4. The detection methods of organic molecules by UHPLC

Compound	Mobile phase (MeOH/H₂O, v/v)	Flow rate (mL·min⁻¹)	Wavelength (nm)	Column
FFA	5/95	1.0	219	C18, 4.6 × 100 mm, 3.5 μM particle size
aniline	60/40	0.2	263	C18, 2.1 × 50 mm, 1.9 μM particle size
4-CP	50/50	0.2	280	C18, 2.1 × 50 mm, 1.9 μM particle size

References

- S1. P. G. Tratnyek, J. Holgné, Oxidation of substituted phenols in the environment - A QSAR analysis of rate constants for reaction with singlet oxygen. *Environ Sci Technol* **25**(9), 1596-1604 (1991).
- S2. D. Kavitha, C. Namasivayam, Experimental and kinetic studies on methylene blue adsorption by coir pith carbon. *Bioresource Technol* **98**(1), 14-21 (2007).
- S3. A. U. Khan, M. Kasha, Singlet molecular oxygen in the Haber-Weiss reaction. *Proc Natl Acad Sci USA* **91**(26), 12365-12367 (1994).
- S4. D. A. Svistunenko, M. A. Sharpe, P. Nicholls, M. T. Wilson, C. E. Cooper, A new method for quantitation of spin concentration by EPR spectroscopy: application to methemoglobin and metmyoglobin. *J Magn Reson* **142**(2), 266-275 (2000).
- S5. U. A. Hellmich, *et al.*, Probing the ATP hydrolysis cycle of the ABC multidrug transporter LmrA by pulsed EPR spectroscopy. *J Am Chem Soc* **134**(13), 5857-5862 (2012).
- S6. A. Schick, H. Rager, Integration of EPR spectra. *Appl Magn Reson* **4**(3), 367-375 (1993).
- S7. S. Halladja, A. T. Halle, J. Aguer, A. Boulkamh, C. Richard, Inhibition of humic substances mediated photooxygenation of furfuryl alcohol by 2,4,6-trimethylphenol. Evidence for reactivity of the phenol with humic triplet excited states. *Environ Sci Technol* **41**(17), 6066-6073 (2007).
- S8. A. M. Braun, *et al.*, (2+4)-Cycloaddition with singlet oxygen. 17O-investigation of the reactivity of furfuryl alcohol endoperoxide. *Photochem Photobiol* **70**(6), 868-874 (1999).
- S9. R. Zboril, M. Mashlan, D. Petridis, Iron(III) oxides from thermal processes-synthesis, structural and magnetic properties, Mössbauer spectroscopy characterization, and applications. *Chem Mater* **14**(3), 969-982 (2002).
- S10. G. Fierro, G. Moretti, G. Ferraris, G. B. Andreozzi, A Mössbauer and structural investigation of Fe-ZSM-5 catalysts: Influence of Fe oxide nanoparticles size on the catalytic behaviour for the NO-SCR by C₃H₈. *Appl Catal B Environ* **102**(1-2), 215-223 (2011).
- S11. X. Li, *et al.*, Excellent photo-Fenton catalysts of Fe-Co Prussian blue analogues and their reaction mechanism study. *Appl Catal B Environ* **179**, 196-205 (2015).
- S12. X. Li, *et al.*, Unique role of Mössbauer spectroscopy in assessing structural features of heterogeneous catalysts. *Appl Catal B Environ* **224**, 518-532 (2018).
- S13. H. Schmidt, A. Al-Ibrahim, U. Dietzel, L. Bieker, The acridine and thiazine dye sensitized photodynamic inactivation of lysozyme - singlet oxygen self-quenching by the sensitizers. *Photochem Photobiol* **33**, 127-130 (1980).
- S14. C. Tanielian, L. Golder, C. Wolff, Production and quenching of singlet oxygen by the sensitizer in dye-sensitized photo-oxygenations. *J Photochem* **25**(2), 117-125 (1984).
- S15. F. Wilkinson, W. P. Helman, A. B. Ross, Rate constants for the decay and reactions of the lowest electronically excited singlet state of molecular oxygen in solution. An expanded and revised compilation. *J Phys Chem Ref Data* **24**(2), 663-1021 (1995).
- S16. K. Mukai, S. Nagai, K. Ohara, Kinetic study of the quenching reaction of singlet oxygen

- by tea catechins in ethanol solution. *Free Radical Bio Med* **39**(6), 752-761 (2005).
- S17. M. J. Thomas, C. S. Foote, Chemistry of singlet oxygen. XXVI. Photooxidation of phenols. *Photochem Photobiol* **27**(6), 683-693 (1977).
- S18. J. Al-Nu'Airat, M. K. Altarawneh, X. Gao, P. R. Westmoreland, B. Z. Dlugogorski, Reaction of aniline with singlet oxygen ($O_2^1\Delta_g$). *J Phys Chem A* **121**, 3199-3206 (2017).
- S19. B. Stevens, S. R. Perez, J. A. Ors, Photoperoxidation of unsaturated organic molecules. XIV. $O_2^1\Delta_g$ acceptor properties and reactivity. *J Am Chem Soc* **96**(22), 6846-6850 (1974).
- S20. A. L. Boreen, B. L. Edhlund, J. B. Cotner, M. N. Kristopher, Indirect photodegradation of dissolved free amino acids: the contribution of singlet oxygen and the differential reactivity of DOM from various sources. *Environ Sci Technol* **42**(15), 5492-4598 (2008).
- S21. W. R. Haag, J. R. Hoigne, E. Gassman, A. M. Braun, Singlet oxygen in surface waters - Part I: Furfuryl alcohol as a trapping agent. *Chemosphere* **13**(5), 631-640 (1984).
- S22. P. Krystynik, *et al.*, Semi-pilot scale environment friendly photocatalytic degradation of 4-chlorophenol with singlet oxygen species-Direct comparison with H_2O_2 /UV-C reaction system. *Appl Catal B Environ* **160**, 506-513 (2014).
- S23. B. F. Sels, D. E. De Vos, P. A. Jacobs, Kinetics of the oxygenation of unsaturated organics with singlet oxygen generated from H_2O_2 by a heterogeneous molybdenum catalyst. *J Am Chem Soc* **129**(21), 6916-6926 (2007).
- S24. A. D. Bokare, W. Choi, Singlet-oxygen generation in alkaline periodate solution. *Environ Sci Technol* **49**(24), 14392-14400 (2015).
- S25. Y. Zhou, *et al.*, Activation of peroxymonosulfate by benzoquinone: A novel nonradical oxidation process. *Environ Sci Technol* **49**(21), 12941-12950 (2015).
- S26. R. M. Cory, *et al.*, Singlet oxygen in the coupled photochemical and biochemical oxidation of dissolved organic matter. *Environ Sci Technol* **44**(10), 3683-3689 (2010).
- S27. W. Hui, *et al.*, Ultrathin black phosphorus nanosheets for efficient singlet oxygen generation. *J Am Chem Soc* **137**(35), 11376-11382 (2015).
- S28. J. D. L. And, H. Gallard, Catalytic decomposition of hydrogen peroxide by Fe(III) in homogeneous aqueous solution: mechanism and kinetic modeling. *Environ Sci Technol* **33**(16), 2726-2732 (1999).
- S29. R. Chen, J. Pignatello, Role of quinone intermediates as electron shuttles in Fenton and photoassisted Fenton oxidations of aromatic compounds. *Environ Sci Technol* **31**(8), 2399-2406 (1997).
- S30. J. J. Pignatello, E. Oliveros, A. MacKay, Advanced oxidation processes for organic contaminant destruction based on the Fenton reaction and related chemistry. *Crit Rev Environ Sci Technol* **36**(1), 1-84 (2006).
- S31. B. H. J. Bielski, Reactivity of HO_2/O_2^- radicals in aqueous solution. *J Phys Chem Ref Data* **14**, 1041-1100 (1985).